Using a 3-D spherical plasmoid to interpret the Sun-to-Earth propagation of the 4 November 1997 coronal mass ejection event

Y. F. Zhou,[1] X. S. Feng,[1] S. T. Wu,[2] D. Du,[3] F. Shen,[1] and C. Q. Xiang[1]

Received 15 December 2010; revised 13 October 2011; accepted 22 October 2011; published 10 January 2012.

[1] We present the time-dependent propagation of a Sun-Earth connection event that occurred on 4 November 1997 using a three-dimensional (3-D) numerical magnetohydrodynamics (MHD) simulation. A global steady state solar wind for this event is obtained by a 3-D SIP-CESE MHD model with Parker's 1-D solar wind solution and measured photospheric magnetic fields as the initial values. Then, superposed on the quiet background solar wind, a spherical plasmoid is used to mimic the 4 November 1997 coronal mass ejection (CME) event. The CME is assumed to arise from the evolution of a spheromak magnetic structure with high-speed, high-pressure, and high-plasma-density plasmoid near the Sun. Moreover, the axis of the initial simulated CME is put at S14W34 to conform to the observed location of this flare/CME event. The result has provided us with a relatively satisfactory comparison with the Wind spacecraft observations, such as southward interplanetary magnetic field and large-scale smooth rotation of the magnetic field associated with the CME.

Citation: Zhou, Y. F., X. S. Feng, S. T. Wu, D. Du, F. Shen, and C. Q. Xiang (2012), Using a 3-D spherical plasmoid to interpret the Sun-to-Earth propagation of the 4 November 1997 coronal mass ejection event, *J. Geophys. Res.*, *117*, A01102, doi:10.1029/2010JA016380.

1. Introduction

[2] Coronal mass ejection (CME) is one of the most frequently eruptive phenomena in the solar atmosphere, which causes significant changes in coronal structure accompanied by observable mass outflow. CMEs, their interplanetary manifestations (Interplanetary coronal mass ejections (ICMEs), including their shocks) and vast structures of plasma and magnetic fields that are expelled from the Sun outward through the heliosphere are now known to be a key causal link between solar eruptions and major interplanetary and geomagnetic disturbances [*Dryer*, 1994]. The geoeffective magnetic field associated with the CME may result from the distortion and amplification of the ambient interplanetary magnetic field (IMF), or the manifestation of coronal magnetic ejecta reaching the Earth in the form of a magnetic cloud. Magnetic clouds have the properties of a strong magnetic field (relative to the ambient IMF), smooth magnetic field rotation and low temperature [*Burlaga et al.*, 1981]. In addition to the IMF factor, non-recurrent goemagnetic storms may be caused by a pressure increase associated with the CME-driven shocks, which can significantly compress the magnetosphere and be as geoeffective as strong sustained southward IMF.

[3] The problem of CME propagation from the Sun to Earth or beyond is one component of space weather that concerns the physical conditions and dynamics of the coupled system comprising the Sun, solar wind, magnetosphere, ionosphere and thermosphere. In order to realistically reflect the 3D characteristics of CME propagation and its interaction with the structured solar wind, as reviewed by *Dryer* [2007] and *Feng et al.* [2011a], the numerical 3D MHD simulation has become one of key problems in modeling space weather events. A number of theoretical models have been proposed to explain the eruption and evolution of CMEs near the Sun, e.g., the photospheric converging and shear motions [*Forbes et al.*, 1994; *Mikic and Linker*, 1994; *Antiochos et al.*, 1994], flux emergence [*Feynman and Martin*, 1995; *Chen and Shibata*, 2000], and flux cancelation [*Zhang et al.*, 2001], although there is no general consensus yet on the triggering mechanism. In practice of numerical study for space weather events, several mechanisms have been proposed to simulate the 3D propagation process of CME in interplanetary space during the last decade, such as density(pressure) or velocity-driven model [*Odstrcil and Pizzo*, 1999; *Groth et al.*, 2000; *Odstrcil et al.*, 2004; *Odstrcil and Pizzo*, 2009; *Hayashi et al.*, 2006; *Shen et al.*, 2007, 2009;*Wu et al.*, 2007; *Zhou et al.*, 2008; *Zhou and Feng*, 2008], semi-circular flux rope model [*Manchester et al.*, 2004a, 2004b, 2006, 2008; *Cohen et al.*, 2008; *Lugaz et al.*, 2005, 2007, 2010], magnetized plasma blob model [*Detman et al.*, 1991; *Chane et al.*, 2006, 2008], and spheromak-type flux rope model [*Vandas et al.*, 1997, 1998; *Kataoka et al.*, 2009]. Some of these simulations computed the disturbance propagation from near the Sun to 1 AU in the near realistic background solar wind

[1]SIGMA Weather Group, State Key Laboratory of Space Weather, Center for Space Science and Applied Research, Chinese Academy of Science, Beijing, China.
[2]Center for Space Plasma and Aeronomic Research, University of Alabama, Huntsville, Alabama, USA.
[3]National Center for Space Weather, CMA, Beijing, China.

0148-0227/12/2010JA016380

[*Shen et al.*, 2007, 2009; *Wu et al.*, 2007; *Manchester et al.*, 2008; *Cohen et al.*, 2008; *Lugaz et al.*, 2007, 2010]. For a comprehensive survey of theoretical models on the eruption and evolution of CMEs near the Sun, and also 3D process study of CMEs in the interplanetary medium, we can refer to *Feng et al.* [2011a].

[4] It is well known that the solar wind ambient is important in the propagation study of CMEs in interplanetary space. Therefore, we first simulate the solar wind ambient by using 3D SIP-CESE MHD model with the observation-based magnetic field and spherically symmetric Parker solar wind as the initial condition [*Feng et al.*, 2007, 2010; *Zhou et al.*, 2008; *Zhou and Feng*, 2008]. In order to produce the realistic fast and slow solar wind structure, an additional coronal heating input is needed with general agreement, although the entire scenario for the coronal heating/solar wind acceleration is still unknown. The details and history of this subject have been debated by scientists for a long time [e.g., *Barnes*, 1992; *Hollweg and Isenberg*, 2002; *Cranmer*, 2002; *Li et al.*, 2007; *Aschwanden*, 2008; *Lu and Chen*, 2009]. Here, we simply add certain parametric source functions in the energy equation to mimic the effects of coronal heating/solar wind acceleration in order to tentatively reproduce a realistic solar wind.

[5] In this paper, we numerically study the 4 November 1997 CME event by using our 3D SIP-CESE model [*Feng et al.*, 2007, 2010; *Zhou et al.*, 2008; *Zhou and Feng*, 2008]. Since there is no general consensus yet on the triggering mechanism of solar eruptions, we instead assume that the CME has already been initiated. Here, we mimic a CME by a 3D spherical plasmoid with high speed, high pressure and high plasma density initially taken to be out of equilibrium near the solar surface on the observed source location of the flare/CME. As such, the model does not address the question of how such an energetic CME is initiated, but describes the three-dimensional propagation and evolution of the CME event from the low corona to the interplanetary space, by providing the time variation of solar wind parameters and magnetic field, which generally are vital to geospace space weather forecasting.

[6] The organization of the paper is as follows. We give a brief description of observational properties of the CME event in section 2. The MHD model is described in section 3. The spherical plasmoid CME model is displayed in section 4. The simulation results of the background solar wind and the CME event are shown in section 5, which includes a discussion of the CME's propagation and interaction with the background solar wind as well as the comparison of the numerical results with Wind spacecraft observations. Finally, we summarize the results and discuss the capabilities and limitations of the MHD model.

2. Observational Properties of the 4 November 1997 CME Event

[7] The 4 November 1997 CME event was associated with the active region NOAA 8100, where a flare of class 2B/X2.1 began at 0554 UT. The SOHO spacecraft recorded the CME between 0552 and 0608 UT. *Dulk et al.* [1999] and *Eto et al.* [2002] reported that the lift-off time of the CME occurred within a few minutes of the peak time of the impulsive X2/3B flare (S14W34). The CME was of halo type, with a reported angular width of 360 degrees. From the LASCO/SOHO observations, *Dulk et al.* [1999] obtained a speed about 750 km/s in the plane of sky. The CME-caused disturbance, having an average speed 646 km/s from 1 R_s to 1 AU, arrived at Earth and produced a strong shock at 2210 UT on 6 November, about 65 hours after the flare and CME lift-off. About several hours later, the magnetic cloud arrived at 1 AU. In Figure 10, we plot the solar wind bulk velocity, density, proton temperature, magnetic field, and X-, Y-, and Z-components of magnetic field (in geocentric solar ecliptic [GSE] coordinates) by dots for a period of 4 days from November 6 to 10. The shock front is indicated by the solid vertical line. The magnetic cloud, indicated by the two dotted vertical lines following the shock sheath, starts at November 7, 0500 UT and ends at November 8, 1200 UT. Figure 10 shows a typical magnetic cloud: the magnetic field direction varies slowly, the magnetic field strength increases, and density, plasma proton temperature and thermal pressure decrease, i.e., the ejecta is a low-beta plasma. Moreover, the solar wind speed decreases as the ejecta passes.

3. Model Description

[8] In order to simulate the propagation of a CME through the interplanetary space, a representative MHD model of the steady state background solar wind is required. Considering the gravitational force and solar rotation we can write the MHD system for the solar wind governing equations as

$$\frac{\partial \mathbf{U}_1}{\partial t} + (\nabla \cdot \mathbf{F}_1) + (\nabla \cdot \mathbf{G}) = \mathbf{S}_1 \tag{1}$$

where the conservative state vectors $\mathbf{U}_1$ is

$$\mathbf{U}_1 = (\rho, \rho\mathbf{u}, E_1, \mathbf{B}_1)^T \tag{2}$$

$\mathbf{F}_1$ and $\mathbf{G}$ flux tensors having the following form

$$\mathbf{F}_1 = \begin{bmatrix} \rho\mathbf{u} \\ \rho\mathbf{u}\mathbf{u} + \left(p + \frac{1}{2}B_1^2\right)\mathbf{I} - \mathbf{B}_1\mathbf{B}_1 \\ \mathbf{u}\left(E_1 + p + \frac{1}{2}B_1^2\right) - (\mathbf{u}\cdot\mathbf{B}_1) \\ \mathbf{u}\mathbf{B}_1 - \mathbf{B}_1\mathbf{u} \end{bmatrix} \tag{3}$$

$$\mathbf{G} = \begin{bmatrix} 0 \\ (\mathbf{B}_0\cdot\mathbf{B}_1)\mathbf{I} - (\mathbf{B}_0\mathbf{B}_1 + \mathbf{B}_1\mathbf{B}_0) \\ (\mathbf{B}_0\cdot\mathbf{B}_1)\ \mathbf{u} - (\mathbf{u}\cdot\mathbf{B}_1)\mathbf{B}_0 \\ \mathbf{u}\mathbf{B}_0 - \mathbf{B}_0\mathbf{u} \end{bmatrix} \tag{4}$$

and the source $\mathbf{S}_1$ is given by

$$\mathbf{S}_1 = \begin{bmatrix} 0 \\ \rho[\mathbf{g} - \boldsymbol{\Omega}\times(\boldsymbol{\Omega}\times\mathbf{r})] - 2\rho\boldsymbol{\Omega}\times\mathbf{u} \\ \rho\mathbf{u}\cdot[\mathbf{g} - \boldsymbol{\Omega}\times(\boldsymbol{\Omega}\times\mathbf{r})] + S_E \\ 0 \end{bmatrix} - \nabla\cdot\mathbf{B}_1 \begin{bmatrix} 0 \\ \mathbf{B} \\ \mathbf{u}\cdot\mathbf{B}_1 \\ \mathbf{u} \end{bmatrix} \tag{5}$$

where ρ, $\mathbf{u}$, p, $\mathbf{B}$ are mass density, bulk velocity, thermal pressure and magnetic field, respectively. A factor of $1/\sqrt{\mu_0}$ has been absorbed into the definition of $\mathbf{B}$. The angular velocity of solar rotation, $\boldsymbol{\Omega}$, is taken to be 2.8×10^{-6} rad/s, the specific heat ratio γ is assumed to be 1.2, and $\mathbf{g} = -g(\mathbf{r}/r^3)$, where g is the gravitational force at the solar

surface. Then, the variables ρ, $\mathbf{u}$, p, $\mathbf{B}$, $\mathbf{r}$, t, g, and $\mathbf{\Omega}$ can been normalized by the characteristic values ρ_s, a_0, $\rho_s a_0^2$, $\sqrt{\rho_s a_0^2}$, R_s, R_s/a_0, $a_0^2 R_s$, and a_0/R_s where ρ_s and a_0 are the initial values of density and sound speed at the solar surface.

[9] In this paper, we split the full magnetic field $\mathbf{B}$ into a constant potential magnetic field $\mathbf{B}_0$ and a deviation $\mathbf{B}_1$, i.e., $\mathbf{B} = \mathbf{B}_0 + \mathbf{B}_1$ [e.g., *Oginio and Walker*, 1984; *Tanaka*, 1994; *Powell et al.*, 1999; *Nakamizo et al.*, 2009; *Feng et al.*, 2010]. Magnetic field $\mathbf{B}_0$ satisfies

$$\frac{\partial \mathbf{B}_0}{\partial t} = 0, \nabla \cdot \mathbf{B}_0 = 0, \nabla \times \mathbf{B}_0 = 0 \tag{6}$$

Gombosi et al. [2003] believed that the splitting is most important when the equations are solved in a (near) conservation form, and the negative pressure can be effectively avoided by rewriting the energy equation in terms of the modified total energy density $E_1 = p/(\gamma - 1) + \frac{1}{2}\rho \mathbf{u} \cdot \mathbf{u} + \frac{1}{2}\mathbf{B}_1 \cdot \mathbf{B}_1$. The source terms involving $\nabla \cdot \mathbf{B}$ may be added to the momentum, induction and energy equations in order to reduce the unphysical effects due to the nonzero divergence of the magnetic field. Usually, in order to keep $\nabla \cdot \mathbf{B}$ to an allowable numerical error, some special treatments, such as the constrained transport (CT) approach, generalized Lagrange multiplier (GLM) method, and the projection method, have been required in finite volume or finite difference schemes [e.g., *Brackbill and Barnes*, 1980; *Evans and Hawley*, 1988; *Toth*, 2000; *Toth et al.*, 2006; *Dedner et al.*, 2002; *Balsara and Kim*, 2004; *Feng et al.*, 2006b, 2010; *Stone and Gardiner*, 2009; *Kleimann et al.*, 2009; *Mignone and Tzeferacos*, 2010; *Yalim et al.*, 2011]. But the CESE scheme can maintain $\nabla \cdot \mathbf{B}$ numerical error in a limited range and do a good work without any special treatment [*Zhang et al.*, 2006; *Feng et al.*, 2006a, 2007; *Qamar and Mudasser*, 2010].

[10] In order to consider the heating/acceleration of the solar wind, we follow the work of [*Nakamizo et al.*, 2009] to define the source term S_E as $S_E = Q \exp(-r/L_Q)$, where Q and L_Q are the intensity and decay length of heating respectively. We take the heating intensity $Q = Q_0 \cdot \frac{1}{f_s}$. The constant value of Q_0 is set to be 1.2×10^{-6} Jm^{-3} s^{-1}, and L_Q is set to be 0.9 R_s. The expansion factor f_s is defined as $f_s = (\frac{R_s}{r})^2 \frac{B_{R_s}}{B_r}$ where R_s and r are 1 solar radius and the distance from the solar center, and B_{R_s} and B_r are magnetic field strength at the solar surface and at r. In the simulation, the expansion factor is time-invariant and same as the value we used during calculating the background solar wind. The involvement of expansion factor in the heating source term is encouraged by the fact that the solar wind speed is inversely correlated with the expansion rate of the magnetic flux tube in the corona [*Levine et al.*, 1977]. *Feng et al.* [2010] designed another kind of volumetric heating and momentum heating method according to the expansion factor and the angular separation between an open field foot point and its nearest coronal hole boundary. In this paper, the parametric source function is only added to the energy equation by involving the topological effect of the magnetic field expansion factor f_s to reproduce the fast and slow solar wind structure.

[11] In this paper, we use the SIP-CESE MHD model [*Feng et al.*, 2007, 2010; *Zhou et al.*, 2008; *Zhou and Feng*, 2008] to compute the quasi-steady solar wind with the observed photospheric magnetic field and Parker's 1D solar wind solution [*Parker*, 1963] as the initial values. The temperature and plasma density at the inner boundary are typically taken to be 1.7×10^6K and $\rho_s = 1.67 \times 10^{-13}$ kgm^{-3} respectively. The initial $\mathbf{B}_1$ is set to be zero, and $\mathbf{B}_0$ is obtained by the potential field source surface (PFSS) model [e.g., *Luhmann et al.*, 2002] based on the observed photospheric magnetic field from the Wilcox Solar observatory at Stanford University (WSO). The computational domain covers $0° \le \theta$ 180°, $0° \le \phi \le 360°$, and $1\ R_s \le r \le 235\ R_s$. The Sun is located at the center of the domain at the origin $(x, y, z) = (0, 0, 0)R_s$. Here, for the analysis of computational results, the corresponding simulated data are transformed to the inertial frame, in which the Earth is fixed at a position $(x, y, z) = (-215, 0, 0)R_s$, i.e., $r = 215\ R_s$, $\theta = 90°$, $\phi = 180°$. The details of computing the background solar wind were given by us [*Feng et al.*, 2007, 2010; *Zhou et al.*, 2008; *Zhou and Feng*, 2008] and thus are omitted here.

4. CME Model

[12] In the present paper, a high speed, high density and high pressure spherical plasmoid is employed to generate the CME. This kind of model is far from being a state-of-the-art CME initiation model with very complex features, but it gives us an easy way to study the evolution and propagation of the CME in the corona and heliospheric space. The density, temperature and radial velocity profile of the initial perturbation are defined as follows:

$$\begin{aligned} \rho &= \rho_0 + \rho_{\max}\left(1 - a^2/a_{\text{cme}}^2\right) \\ T &= T_0 + T_{\max}\left(1 - a^2/a_{\text{cme}}^2\right) \\ v_r &= v_{r0} + v_{\max}\left(1 - a^2/a_{\text{cme}}^2\right) \end{aligned} \tag{7}$$

where a_{cme} is the radius of the plasmoid, a denotes the distance from the center of the plasmoid, and ρ_0, v_{r0} and T_0 are the density, radial velocity, and temperature of the background solar wind. $\rho_{\max}$, $v_{\max}$ and $T_{\max}$ are the maximum density, radial velocity and temperature added on top of the background solar wind, respectively. In order to match the Wind data as the best fit as possible, the choices of these parameters are empirical. The value of $v_{\max}$ is set to be 300 km/s. $\rho_{\max}$ and $T_{\max}$ are assumed to be five and three that of the ambient solar wind at the center of the CME, respectively.

[13] *Gibson and Fan* [2008] believed that the spheroidal magnetic field may be a natural product of a plasmoid ejected from a solar flare via reconnection, although the actual existence in the solar wind is under debate [e.g., *Vandas et al.*, 2002; *Farrugia et al.*, 1995]. Whereas *Wang et al.* [2010a, 2010b] described certain existence evidence on plasmoid in the magnetotail. In the present paper, the initial magnetic field of the spherical plasmoid is assumed to take the spheromak-type magnetic field form as the "classical" spheromak of *Farrugia et al.* [1995] in local spherical coordinates $(r^\ell, \theta^\ell, \phi^\ell)$:

$$\begin{aligned} B_{r^\ell} &= \left(2B_0/\alpha r^\ell\right) j_1\left(\alpha r^\ell\right) cos\theta^\ell \\ B_{\theta^\ell} &= -\left(B_0/\alpha r^\ell\right)\left[sin\left(\alpha r^\ell\right) - j_1\left(\alpha r^\ell\right)\right] sin\theta^\ell \\ B_{\phi^\ell} &= \pm B_0 j_1\left(\alpha r^\ell\right) sin\theta^\ell \end{aligned} \tag{8}$$

where B_0 is a constant, and $\alpha = 4.493409458 a_{\text{cme}}^{-1}$ is the constant derived from the force-free condition of $\nabla \times \mathbf{B} = \alpha \mathbf{B}$

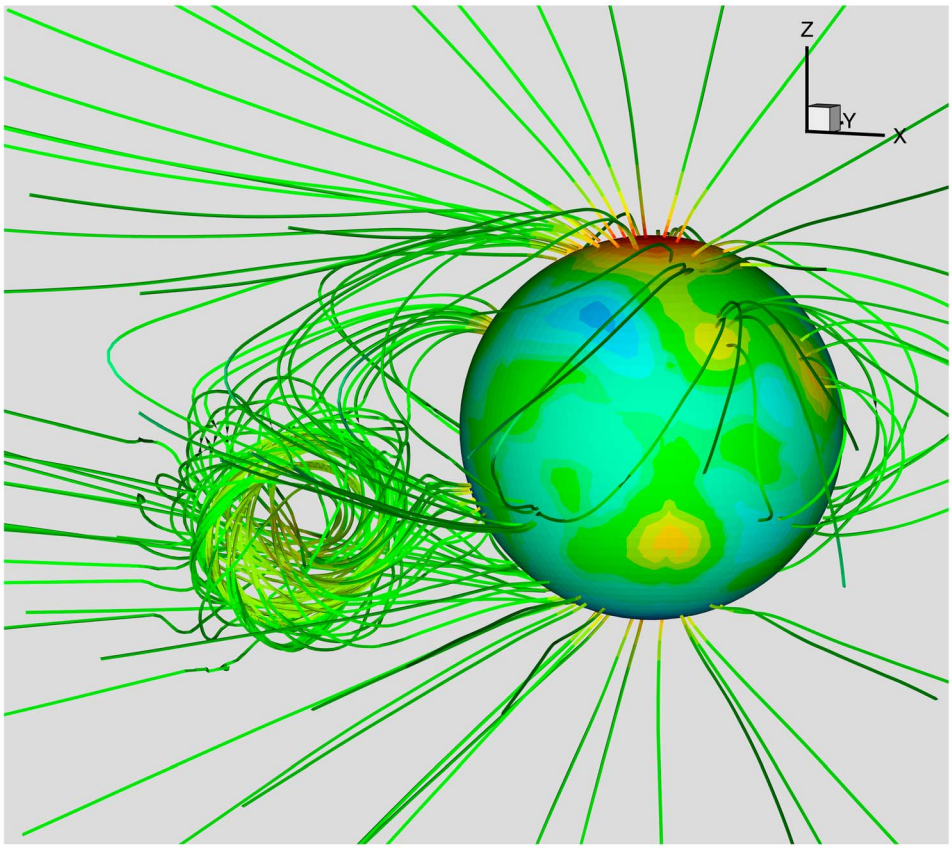

Figure 1. Three dimensional view of the initial coronal magnetic field. Field lines of the CME are shown in color to illustrate the magnetic field strength. The color contours represent the radial magnetic field strength on the solar surface.

with the boundary condition of $B_r^{\ell} = 0$ at $r^{\ell} = a_{\rm cme}$. $j_1(x)$ is the spherical Bessel function, $j_1(x) = x^{-2} \sin x - x^{-1} \cos x$. The parameter α becomes negative for left-handed polarity. The center of the CME is initially placed at 1.8 R_s. The radius of the initial CME, $a_{\rm cme}$, is 0.6 R_s. The maximal magnetic field strength B_0 is 5.0 G. The CME is launched at S14W34 (i.e., $\theta = 104°$, $\phi = 214°$) to conform to the location of the flare/CME. In order to find a better agreement with the in-situ IMF observations, we rotate the polar axis of the ejected spheromak toward the negative y-axis direction, so that the polar axis is inclined about 42 degree from the negative y-axis. During the simulation of the CME event, we have tested various angles, and found that the angle can best match the observed magnetic field. The introduction of the plasma plasmoid to the corona has added 5.77×10^{31} ergs of magnetic energy, 4.33×10^{30} ergs of kinetic and 5.55×10^{31} ergs of thermal energy. The total energy (magnetic + kinetic + thermal energy) increase is 1.75×10^{32} ergs. In the simulation, t=0 is taken to be at 0554 UT on 4 November 1997, when the flare associated with the halo CME was observed from AR 8100. Figure 1 shows the 3D schematic picture of the initial coronal magnetic field at t = 0.

5. Results and Discussion

[14] In this section, we will present the results of the 3D MHD numerical simulation, which include the solar wind ambient obtained from the method of time relaxation, the morphology and propagation of the CME, and the comparison between the numerical results and the in-situ data from Wind.

5.1. The Solar Wind Ambient

[15] Figure 2 shows the background solar wind solution for the experiment of the 4 November 1997 CME event at a solar coronal meridional plane (Figure 2a) and an inner heliosphere solar equatorial plane (Figure 2b) respectively. The color image indicates the radial speed of the plasma while the magnetic field is represented by solid black lines. From Figure 2a, we can see that the magnetic field and radial speed possess a typical characteristic of solar minimum. At lower latitudes around the equator, a helmet streamer with low radial speed is stretched by the solar wind. At high latitudes, the magnetic field is carried out with the solar wind to achieve an open configuration with high radial speed. Figure 2b shows that the IMF lines are stretched by the solar wind outward into Archimedean spirals due to the solar rotation and the IMF freezing-in effect.

[16] Figure 3 shows the steady state background solar wind parameters at 1 AU. The results simultaneously reproduce the high- and low-temperature regions, the fast (low density) and slow(high density) solar wind structure in interplanetary space. From Figure 3, we can found that the

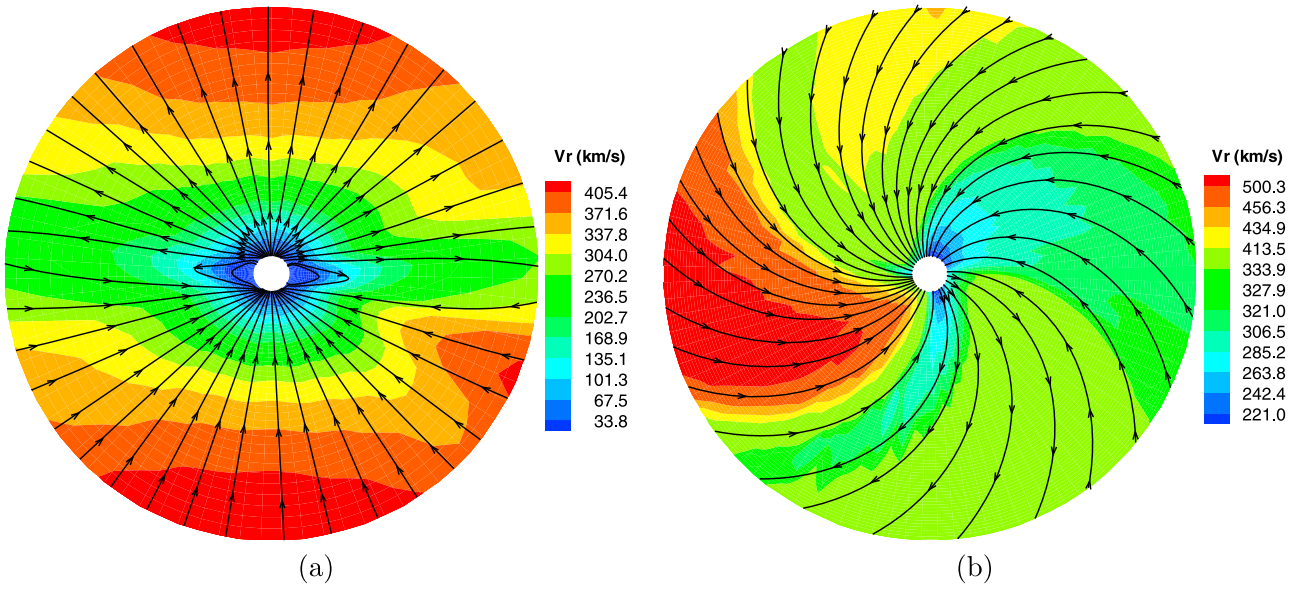

Figure 2. Magnetic field and radial speed for the steady state solar wind solution. (a) Solar coronal solution at ϕ = 180°–0° from $1R_s$ to $15R_s$ and (b) inner heliosphere solution in the solar equatorial plane from $15R_s$ to $215R_s$. The color contours represent the radial speed and streamlines denote the magnetic field lines.

radial speed profile is in agreement on the temperature profile, and inverse against the density profile. Inspection of Figure 3b reveals an approximate bimodal outflow pattern with slow wind leaving the Sun around 350 km/s near the current sheet region and high-speed wind above 600 km/s in the high-latitude region. The variation in the background solar wind in this model results from coronal heating and flux expansion. But we find the radial speed is higher than the observed speed near the Earth, which may be caused by the low expansion factor owing to the contamination of six impulsive solar events in November 1997.

5.2. The Morphology and Propagation of the CME

[17] In Figure 4, we compare the observed and synthetic LASCO C2 and EIT images for the ejection. The top two images are the C2 and EIT running-difference images for the CME. The bottom two images show the corresponding synthetic images. By comparing the simulation results and

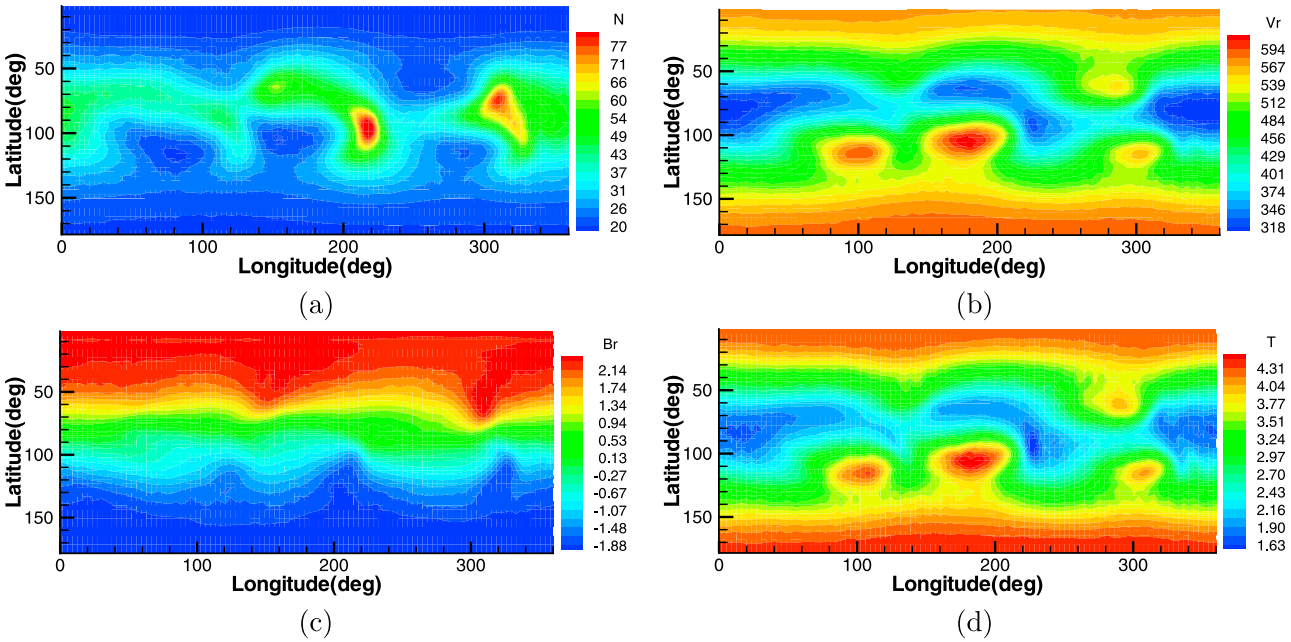

Figure 3. The steady state solar wind parameters at 1 AU. (a) Number density (cm^{-3}) and (b) radial speed (km/s). (c) Radial magnetic field (nT) and (d) plasma temperature (10^5K).

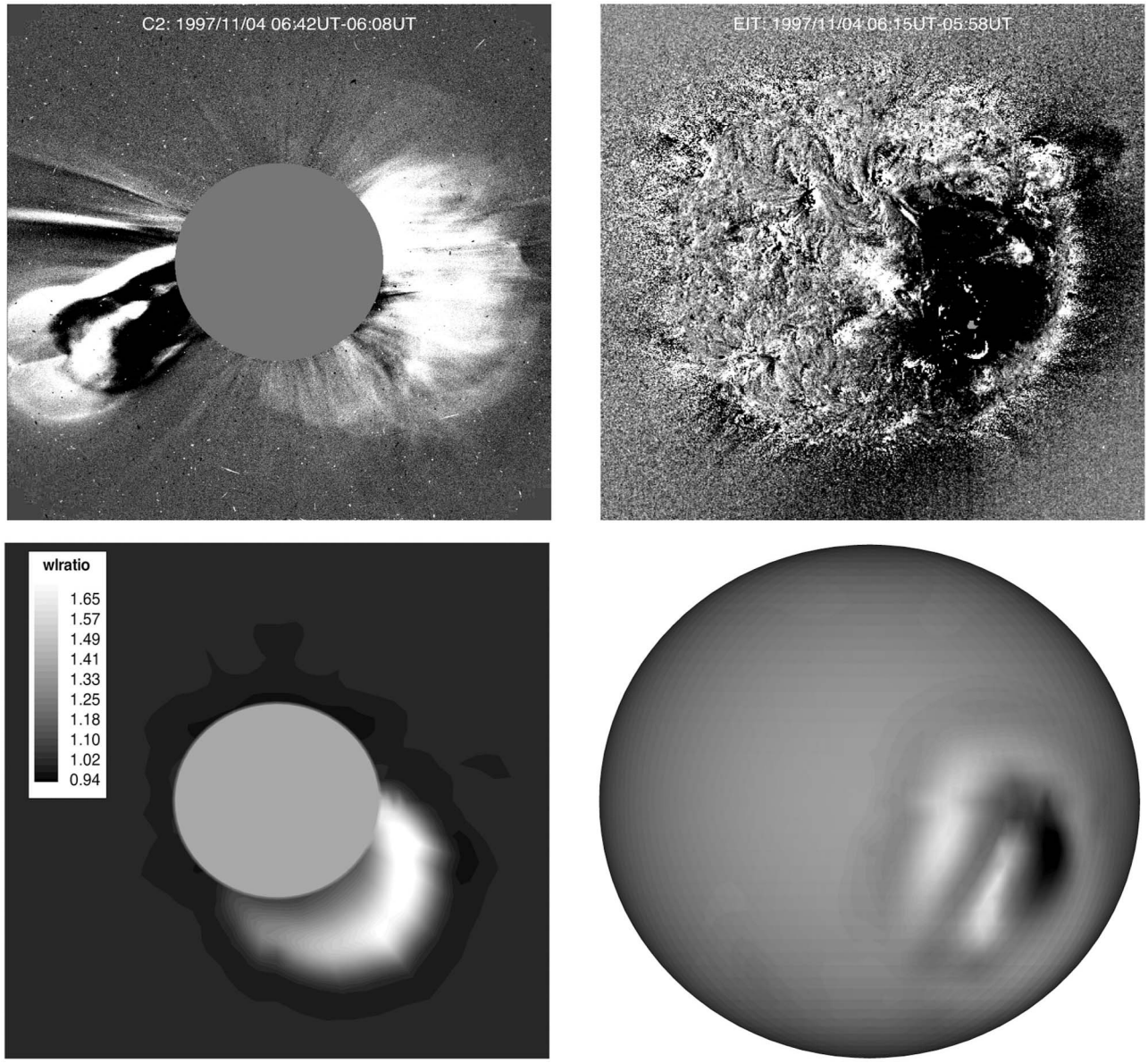

Figure 4. (top) C2 and EIT difference images. (bottom) Synthetic white light running ratio image corresponding to C2 field-of-view (left), numerically simulated density-enhancement image on the solar disk (right).

observations, we can see clearly that the simulated white light image is in good agreement with the observed one, and that the simulated density enhancement compares well with the EIT intensity enhancement.

[18] Figure 5 shows a 3D view of the CME at t = 1.0, 3.0, 5.0, and 10 hours after the initiation. The false color image shows the velocity magnitude in the x-y equatorial plane. The magnetic field of the CME is colored to illustrate the velocity magnitude. The evolution of the CME on the meridional at $\phi = 210°$ is shown in Figure 6 at four different instants (t = 1.0, 3.0, 5.0 and 10.0 hours). Figure 6 depicts the system in 2-D meridional slices (x-z plane) with false color images of the plasma velocity magnitude upon which solid black lines represent the magnetic field. From Figures 5 and 6, we find that initially the magnetic field evolves nearly in self-similar manner. The plasmoid rapidly expands and is expelled from the corona since the injected CME has higher plasma density, speed, and magnetic pressure than the solar wind ambient. The radial and angular sizes of the CME increase with time. The plasma velocity magnitude shows that the evolution of the CME begins with rapid acceleration to a speed over 780 km/s at 7 R_s which almost agrees with the speed in the plane of sky from the LASCO observation, then undergoes a gradual deceleration to a speed of 710 km/s at 42 R_s. In our simulation, most of the magnetic field lines of CME are connected to the inner boundary from the beginning, as shown in Figure 6, since the magnetic field of the spherical plasmoid is introduced by simple superposition on the ambient field.

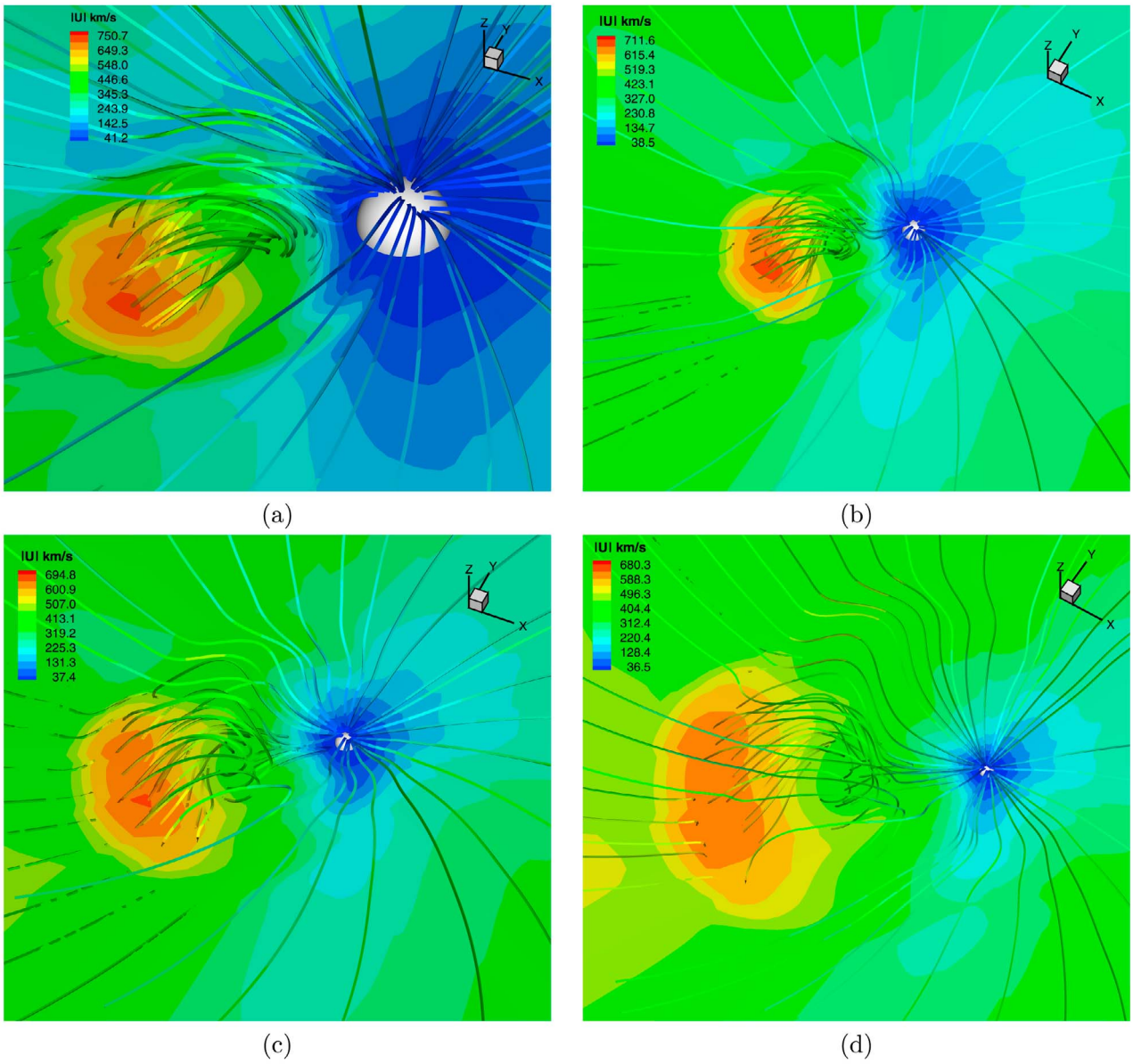

Figure 5. A 3D representation of the CME is shown at (a) 1 hour, (b) 3 hours, (c) 5 hours, and (d) 10 hours after initiation. The color code represents the velocity magnitude in the x-y equatorial plane. Field lines of the CME are shown in color to illustrate velocity magnitude. The Sun is shown with a white sphere.

[19] Figure 7 shows the time profiles for the relative number density, velocity, relative temperature and magnetic field at selected solar radii r_i along $\theta = 0°$, $\phi = 210°$ (Figures 7a–7d) and $\phi = 180°$ (Figures 7e–7h). We find that the overall similarity (such as sharp rise and slow decay of the velocity's maxima, and the sharp jumps of the magnetic field, density and temperature) of the computed time profiles in the inner heliospheric (r_i = 10 R_s, 20 R_s). The forward CME shock is well developed. It originates at the leading edge of the CME due to the collision of high-speed CME plasma with the background slow stream. The distribution of plasma parameters in Figure 7 shows a significant expansion of the CME. As the CME propagates further into interplanetary space(r_i = 50 R_s, 100 R_s), it continues to expand due to the pressure gradients, the difference between the speeds at the leading and trailing edges decreases, and velocity's maxima also decrease. Simultaneously, we can find that the variation amplitude at ϕ = 180° is smaller than that at ϕ = 210°, especially the difference of the magnetic field is more obvious. The arrival time of the disturbance at the same heliocentric distance at ϕ = 180° delays a few hours relative to that at ϕ = 210°, and that the farther away from the Sun the disturbance is, the longer the time delay is.

[20] Figure 8 shows the simulated global view of the relative density ($(\rho - \rho_0)/\rho_0$) (Figures 8a–8f) and the velocity (Figures 8g–8i) at 2.0° south, close to the Earth's latitude at different instants, where ρ is the density, and ρ_0 the density

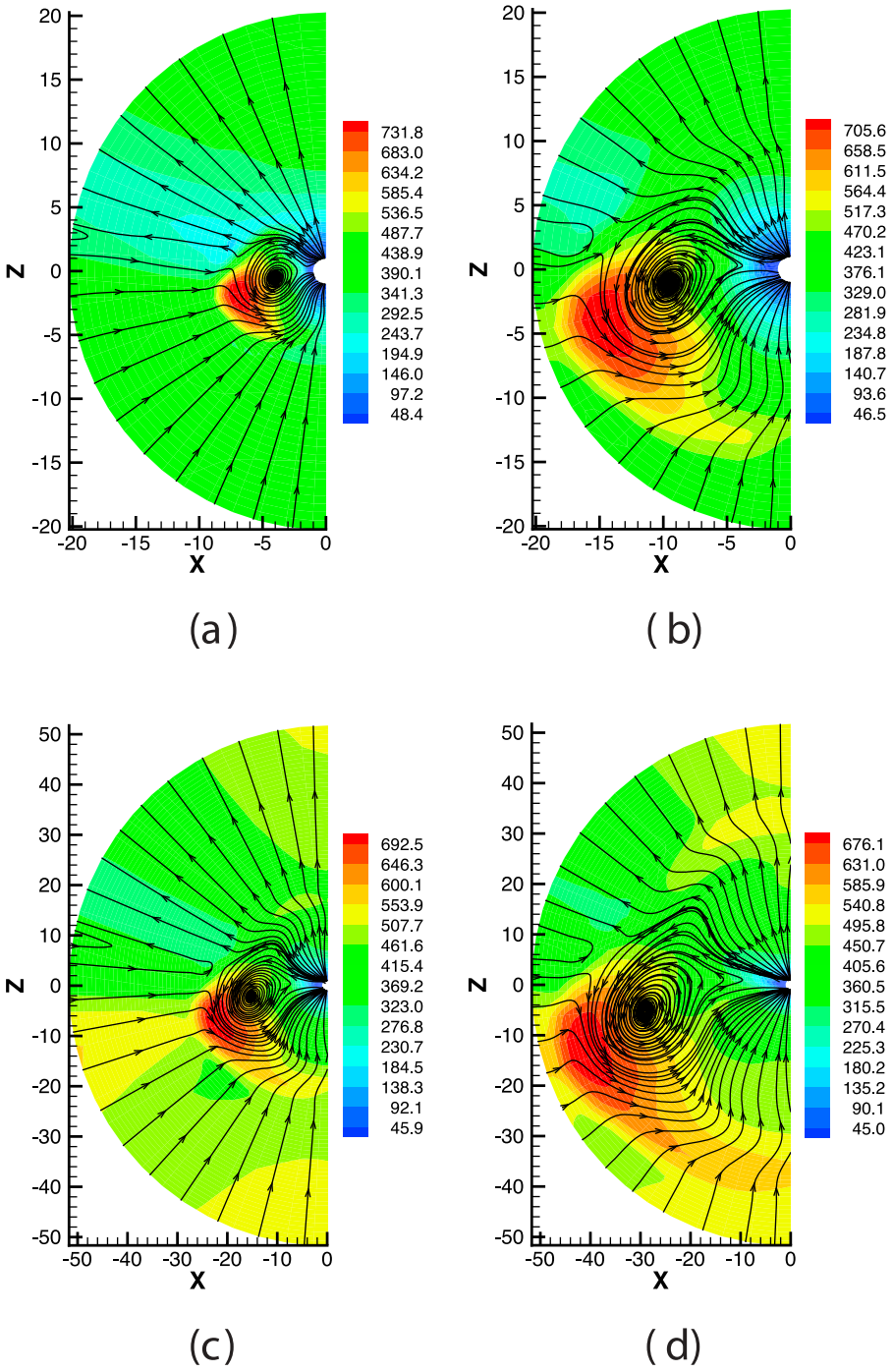

Figure 6. Time evolution of the CME in the x-z meridional plane at (a) t = 1 hour, (b) t = 3 hours, (c) t = 5 hours, and (d) t = 10 hours. Solid black lines display magnetic "streamlines" superimposed upon a false color image of the velocity magnitude.

of the background solar wind. Figures 8a–8c show the domain from 1 to 30 R_s within 5 hours after the initiation, and Figures 8d–8i show views from 1 R_s to 1 AU after 20 hours. From Figure 8, we find that the CME almost propagates along the Parker spiral. There is almost no pronounced eastward deflection of the CME during its outward propagation because of the little speed difference between the CME and the background solar wind, which can be seen in Figures 8g–8i. This is consistent with the observational analyses of the deflection of CMEs' propagation in interplanetary space by *Wang et al.* [2004]. Asymmetry of the CME is clearly seen in heliolongitude as it passes into non-uniform solar wind ambient, and the asymmetry of the CME in heliolatitude can also be seen clearly from Figures 9a, 9b, and 9c.

[21] The evolutions of the CME in interplanetary space at $\phi = 210°$ are displayed in Figure 9 at t=20, 30 and 50 hours after the CME injection. The magnetic field is represented

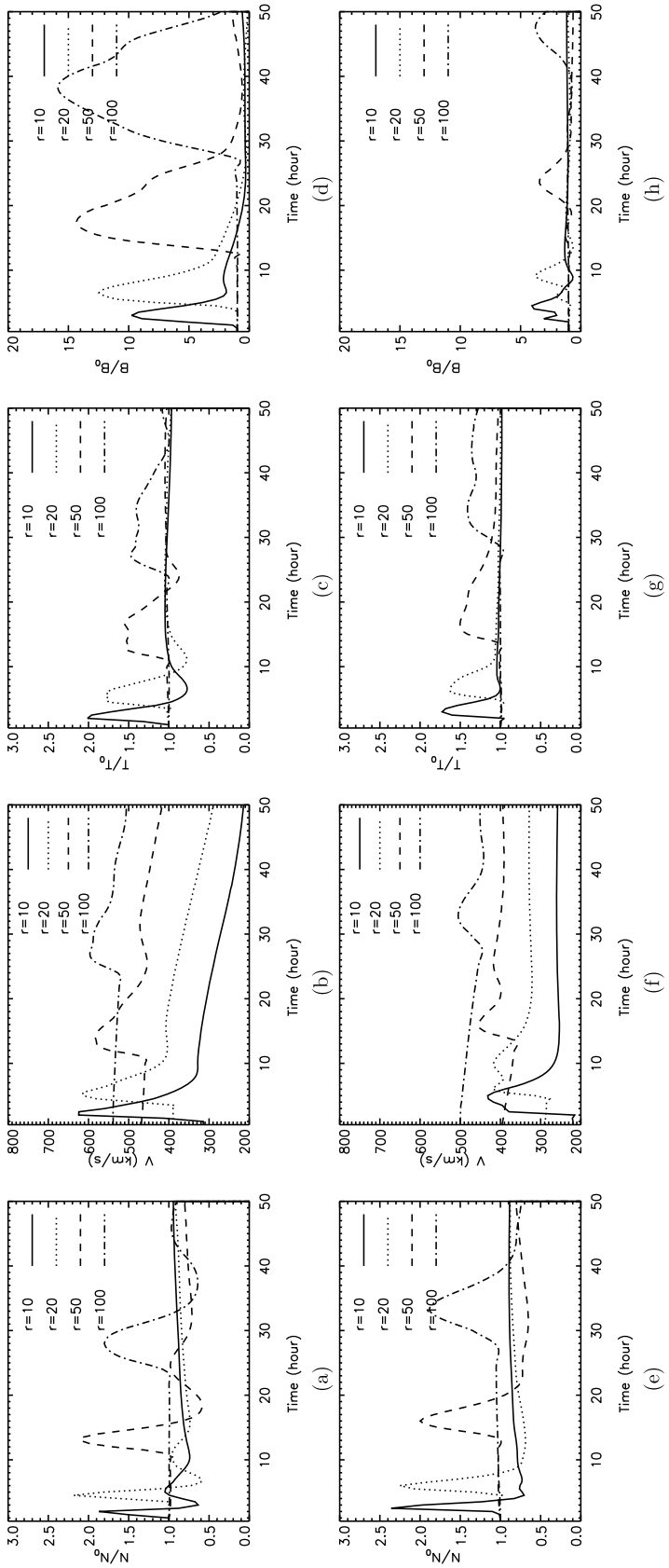

Figure 7. Time profiles for the relative number density N/N_0, velocity V, relative temperature T/T_0, and relative magnetic field B/B_0, at selected solar radii r_i along (a–d) $\theta = 0°$, $\phi = 210°$ and (e–h) $\phi = 180°$. Time is given in hours after the CME onset.

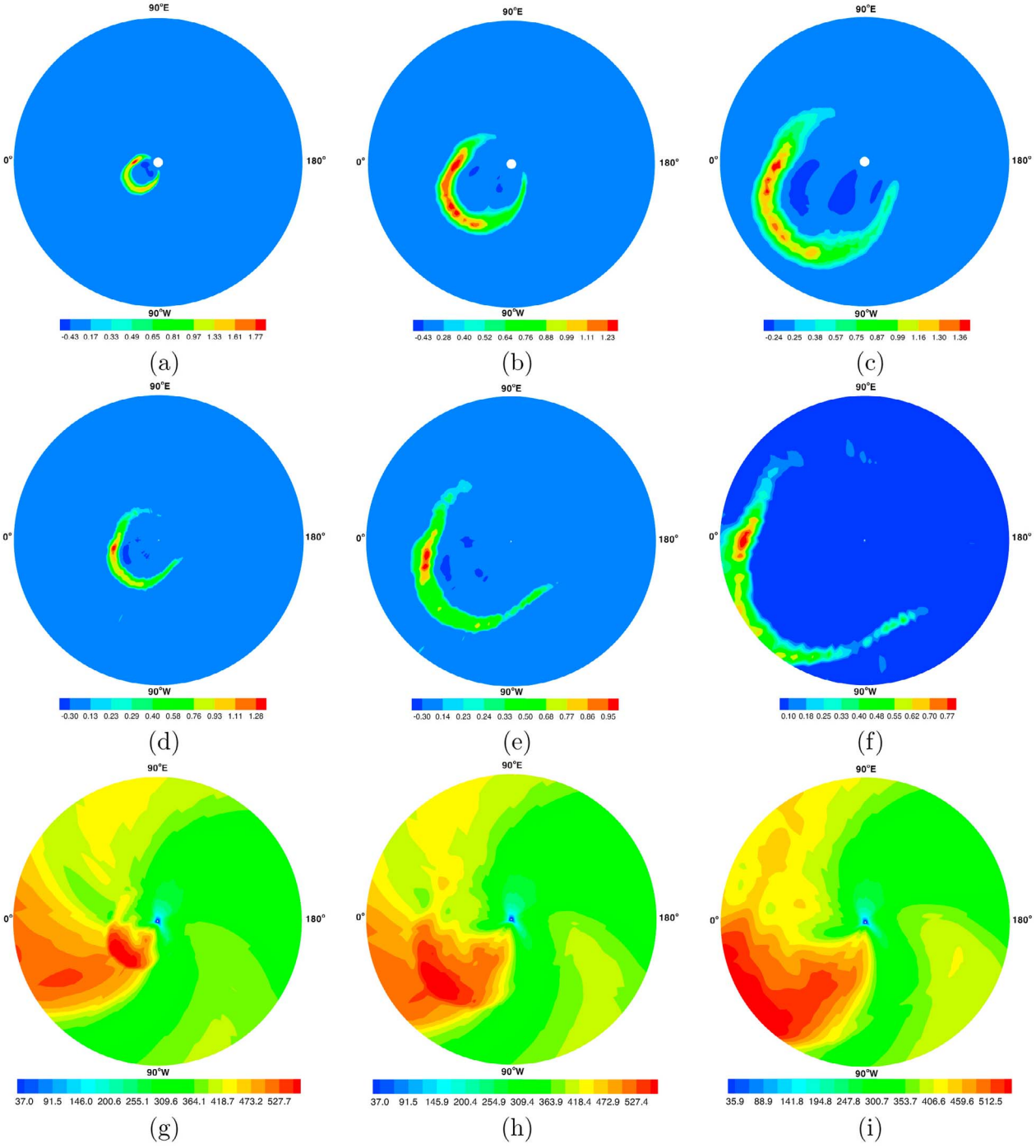

Figure 8. The simulated profiles of the relative density (Figures 8a–8f) and the velocity (Figures 8g–8i) in the x-y azimuthal plane at (a) t = 1 hour, (b) t = 3 hours, (c) t = 5 hours, (d and g) t = 20 hours, (e and h) t = 40 hours, and (f and i) t = 60 hours.

by solid black lines. The false color images of Figures 9a, 9b, and 9c indicate the relative density, while the false color image of Figure 9d indicates the magnetic field strength.

[22] The distribution of the relative density exhibits a concave-outward shape possible stemming either from intrinsic speed gradients within the CME or from the interactions with the structured ambient solar wind. The CME propagates slower near the streamer belt and faster in the open field region. Near the streamer belt, the CME plows most directly into the slow, dense streamer belt flow, its excess momentum is quickly dissipated, a compression is built up at its front, and the disturbance abruptly decelerates. By contrast, the open-field extensions of the CME are pulled rapidly outward by the fast flow toward the poles. *Riley et al.* [1997] suggested that the observations were indicative of a strong velocity shear between Ulysses and Geotail

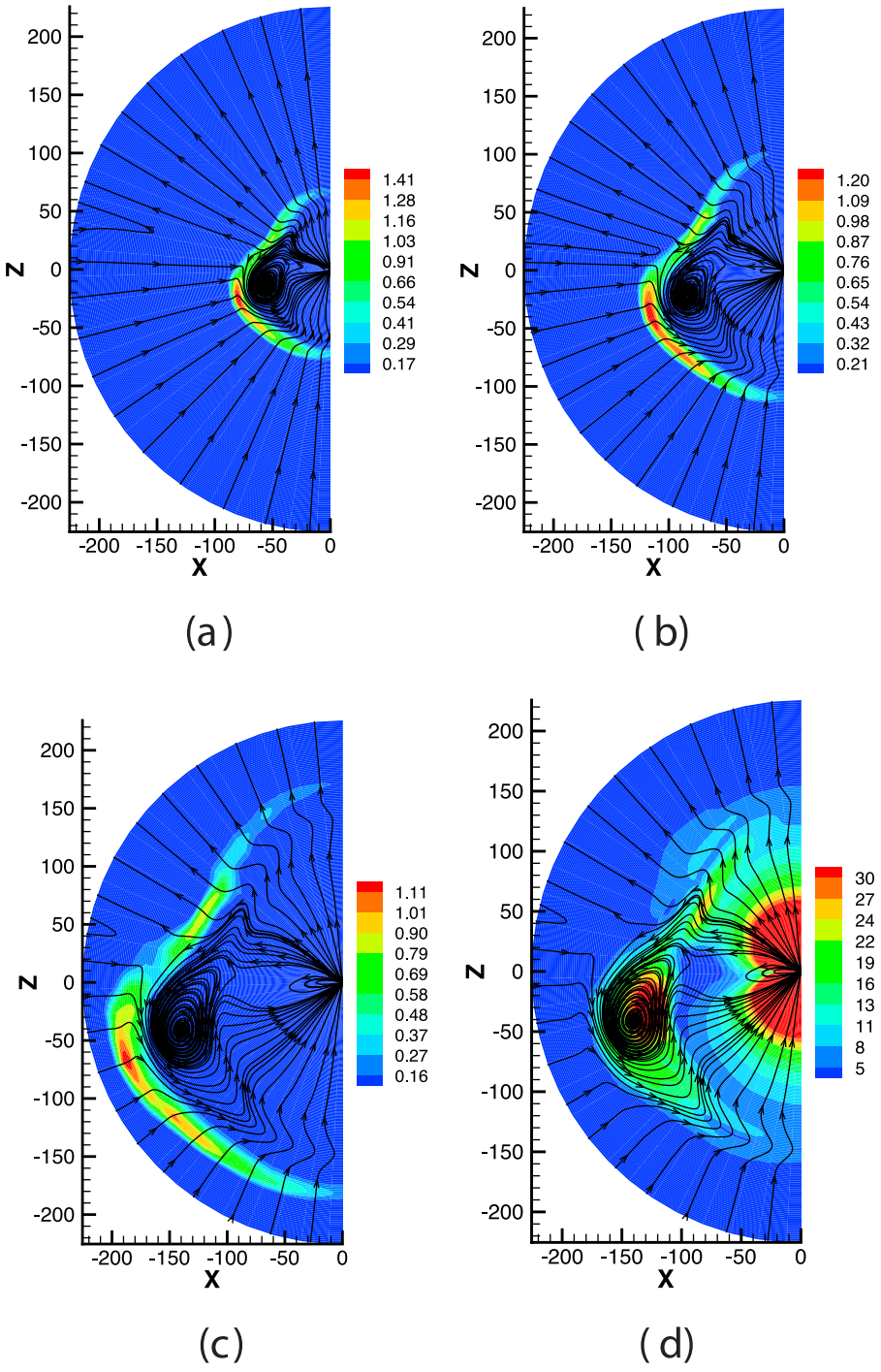

Figure 9. Global view of the CME interaction with the background solar wind in interplanetary space at $\phi = 210°$ and different times: (a) t = 20 hours, (b) t = 30 hours, and (c and d) t = 50 hours. Solid black lines display magnetic "streamlines". Figures 9a, 9b, and 9c show the false color images of the relative density, while Figure 9d shows the false color images of the magnetic field strength.

spacecraft, with the CME being launched such that one part was in a high speed stream while the other part was in a slow stream.

[23] The radial and meridional width of the CME increases with distance. But the rate of radial expansion slowly decreases as the CME is expanding. The initially circular magnetic field gradually distorts owing to its interaction with a slower solar wind ambient. It expands latitudinally while being squeezed radially. Thus the initial circular shape has evolved into an elliptical, lentil-like one and that while the leading edge is still curved, the trailing edge has been flattened. Such shape changes have also been observed in other numerical simulations [*Odstrcil et al.*, 2002; *Cargill and Schmidt*, 2000] due to the different hydrodynamic forces

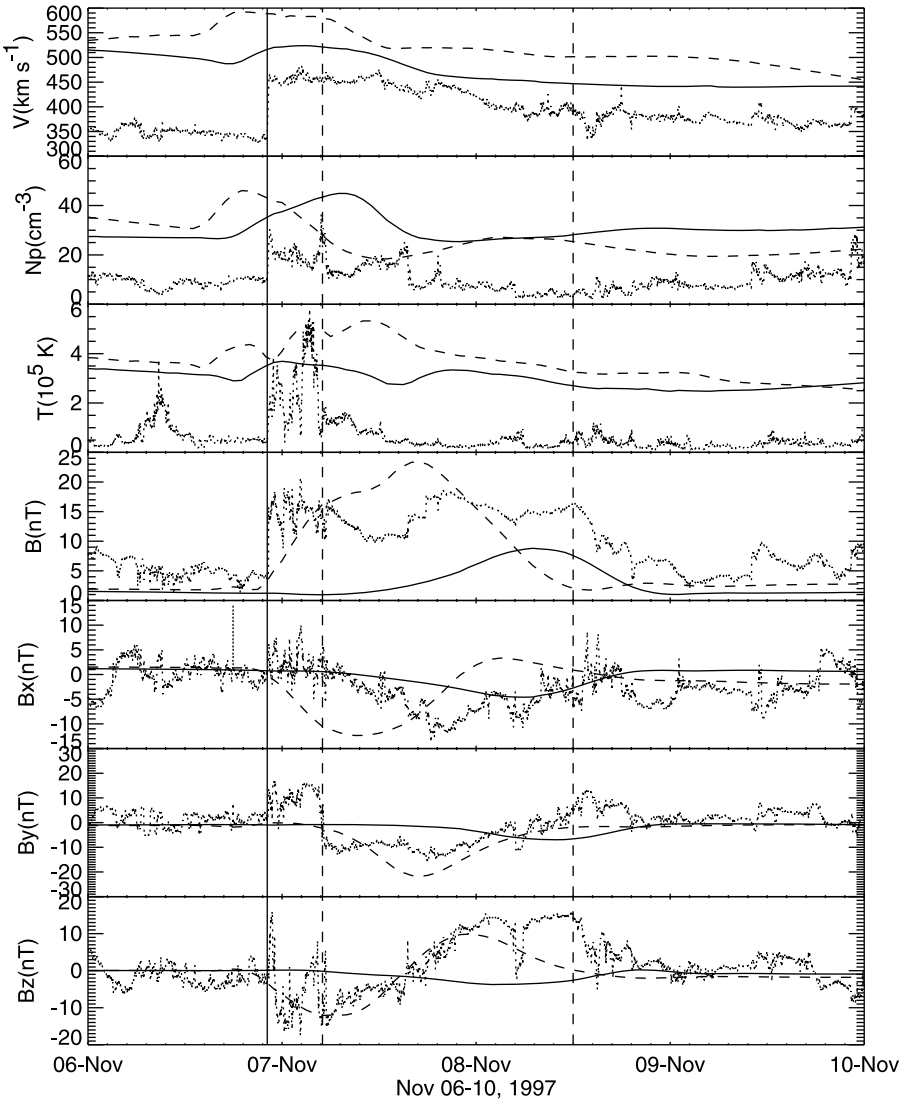

Figure 10. Evolution of solar wind parameters at the Earth during the 04 Nov 1997 event. Shown are flow velocity, number density, temperature, magnetic field, and three components of magnetic field in GSE coordinates. The simulated results at the Earth are shown by solid lines. The Wind observations are shown by dots. The dashed lines show the solar wind profile computed at a position 30 deg westward of the Earth.

acting on each side. At t = 50 hours, the numerical simulation shows that the trailing part of the magnetic field begins to flatten noticeably. As the CME expands, each part of its surface pushes against different plasma conditions. Since the pressure and density at the rear are higher than those at the front, the expansion will be inhibited at the rear relative to the front. This is also a feature of 1D models [*Gosling et al.*, 1998; *Riley et al.*, 2001]. While moving around the boundary from the rear to the sides, the expansion gradually encounters the regions of lower external plasma pressure and density so that the expansion becomes easier. Since the rear part of the CME expands by different distances while going around the boundary, this cumulative effect leads to the flattened shape. The front of the CME expands more easily than the side parts since it encounters a lower pressure and density.

[24] The compression of the magnetic field is clearly seen on the north in Figure 9d, which is most pronounced where the magnetic field of the CME moves through the dense plasma sheet, but it doesn't penetrate the streamer belt. However, the CME still moves southward until it reaches the boundary of the open field with high speed. This may be caused by the higher thermal and magnetic pressure at the faster solar wind region.

5.3. Comparison With in Situ Data

[25] To make a comparison with in situ measurements, Figure 10 simultaneously shows the computed plasma parameters at the Earth and its 30 deg westward and Wind observations for the same time interval. From Figure 10, we find that the simulated solar wind parameters at 30 deg westward of the Earth can better reproduce many basic

structures: such as an increase in the magnetic field magnitude, the behaviors of three components of magnetic field, in particular southward B_z and the large-scale smooth magnetic field rotation. The discrepancy may result from the following factors such as the less accurate distribution of the initial disturbancethe inadequate expansion owing to the less realistic solar wind ambient, and almost no deflection of the CME due to the small speed difference between the CME and the solar wind ambient. For a better comparison with the Wind observation, we shift 4 hours ahead to the time axis of simulated profiles and multiply the computed magnetic field by 2 just because the computed magnetic field is nearly half of that by observation.

[26] From Figure 10, we can see that the simulated background velocity and density at the Earth is higher, the magnetic field is smaller than those by observation. The simulated plasma density is 3–4 times large, and the simulated velocity is almost 150 km s^{-1} greater than that by observation. The reason for this may be due to the single fluid model used, the volumetric heating assumption and other reasons as pointed out by *Feng et al.* [2010]. In this paper, the choice of such a heating may obtain a typical background solar wind characteristic of solar minimum due to the consideration of magnetic field topology. To further understand this problem, more observations of multiple spacecraft (such as SDO, STEREO, SOHO, ACE, Wind, or other future missions) will probably help us develop the ability of including physically realistic coronal heating modules into 3D MHD codes, improve the determination of the structure of the ambient solar wind, and further numerically characterize the 3D propagation of CMEs through the heliosphere.

[27] From the computed B_z at 30 deg westward of the Earth shown in Figure 10, we find that the field turns southward at ~1800 UT on 6 November 1997 for nineteen hours, reaching a minimum -6 nT. The magnetic field then smoothly rotates northward reaching a similar magnitude, lasting more than twenty hours. This magnetic field south-north rotation is mainly due to the passage through the helical field of the CME mentioned by [*Wu et al.* [1999]. The strong southward to northward turning of the IMF and prolonged southward IMF shown in this paper can produce a strong magnetospheric response. But the magnetic field of our model at 1 AU has nearly 50% magnetic magnitude of the observed magnetic cloud. The reason for this may be also due to the small background magnetic field caused by the imperfectness of potential field source surface model and the coarse grid resolution in interplanetary space.

6. Conclusions

[28] We have used our 3D SIP-CESE MHD model to investigate the temporal and spatial evolution of 4 November 1997 CME event from near the Sun to 1 AU. Our results show that early evolution of the CME is nearly self-similar, but a consequence of the combined effects of radial flow collision, lateral material expansion, velocity and pressure gradients within the realistic background solar wind, and the interaction with the background solar wind structure eventually distort the CME. We follow the propagation of the CME to 1 AU and examine the time evolution of plasma properties. We find that the simulated result at 30 deg westward of the Earth is in better agreement with Wind observation than that at the Earth, such as the large increase in magnetic field strength, large-scale magnetic field rotation and prolonged southward IMF.

[29] In our simulations, the CME event is launched at S14W34 to conform to the observed location of the flare/CME. Initially, the CME is out of equilibrium with its surroundings with higher magnetic pressure and internal pressure. The CME rapidly expands from near the Sun, and its volume significantly increases with time. Then, after a short distance from the inner boundary, the CME undergoes a compression. This expansion decelerates with distance and ends until a pressure equilibrium is established. Because of fast outflow over the poles and slow outflow near the streamer belt, the parts of the CME in the originally open-field regions tend to travel faster than the near-streamer belt part. As the CME pushes through the center of the slow, dense streamer belt flow, a compression is built up at its front to form a concave-outward shape, and the disturbance abruptly decelerates.

[30] To sum up, our present study can match some observations from Wind, although a very simple 3D spherical plasmoid model is used to generate the CME. This simulation represents an ongoing effort to develop global space weather models that can track the initiation of CMEs, follow their propagation in interplanetary space, and accurately predict plasma properties at 1 AU that subsequently impact on the Earth's magnetosphere. Although the simulation has reproduced some features of the CME, there is a long way for the model to predict the specific Sun-Earth connection events with an acceptable accuracy. The first point under consideration to improve our model is to tune the parameters of the perturbation more carefully. Our tests have found that the perturbed amplitude of the plasma temperature is the most sensitive factor of the CME's speed and that of magnetic field is the second most sensitive factor. However, the CME's speed is least sensitive to the perturbation amplitudes of density and velocity. These conclusions are similar to those made by *Wu et al.* [2005], who gave very detailed discussions about the difference between the simulation results with different choices of parameters. Thus we should seek the optimal choice of these parameters in order to settle a compromise among different observations. The second point is to make use of multiple observations to determine the orientation of the polar axis and the location of the ejected spheromak [e.g., *Lynch et al.* 2010], which are also very important to make the simulation results closer to interplanetary in-situ measurements. The third way is to absorb the recent effort of our research group in investigating the more realistic solar wind background [*Feng et al.*, 2010, 2011b; *Yang et al.*, 2011], which is achieved by adjusting the empirical terms of coronal heating and solar wind acceleration in the MHD equations and employing other numerical techniques.

[31] **Acknowledgments.** The work is jointly supported by the National Natural Science Foundation of China (40921063, 40890162, 41031066, 40904050, 40874077, 40874091, and 40804029), and the Specialized Research Fund for State Key Laboratories. S. T. Wu is supported by AFOSR (grant FA9550-07-1-0468), AURA Sub-Award C10569A of NSO's Cooperative Agreement AST 0132798, and NSF (grant ATM-0754378). We thank the SOHO/LASCO team for letting us use their data. SOHO is a mission of international collaboration between ESA and NASA. The Wilcox Solar Observatory data used in this study were obtained via the

Web site http://wso.stanford.edu at 2009:05:06_17:15:30 PDT courtesy of J. T. Hoeksema. The Wilcox Solar Observatory is currently supported by NASA. We also thank OmniWeb, http://omniweb.gsfc.nasa.gov/, from which we downloaded the hourly average solar wind data by Wind. The numerical calculation was completed on our SIGMA Cluster computing system. Special thanks go to our anonymous referee for constructive comments on the improvements of the paper.

[32] Philippa Browning thanks the reviewers for their assistance in evaluating this paper.

References

Antiochos, S. K., R. B. Dahlburg, and J. A. Klimchuk (1994), The magnetic field of solar prominences, *Astrophys. J.*, *420*, L41–L44.

Aschwanden, M. J. (2008), Theoretical modeling for the STEREO mission, *Space Sci. Rev.*, *136*, 565–604.

Balsara, D. S., and J. Kim (2004), A comparison between divergence-cleaning and staggered-mesh formulations for numerical magnetohydrodynamics, *Astrophys. J.*, *602*, 1079–1090.

Barnes, A. (1992), Acceleration of the solar wind, *Rev. Geophys.*, *30*(1), 43–55.

Brackbill, J. U., and D. C. Barnes (1980), The effect of nonzero $\nabla \cdot \mathbf{B}$ on the numerical solution of the magnetohydrodynamic equations, *J. Comput. Phys.*, *35*, 426–430.

Burlaga, L. F., E. Sittler, F. Mariani, and R. Schwenn (1981), Magnetic loop behind an interplanetary shock, *J. Geophys. Res.*, *86*, 6673–6684, doi:10.1029/JA086iA08p06673.

Cargill, P. J., and J. Schmidt (2000), Magnetic structure of overexpanding coronal mass ejections: Numerical model, *J. Geophys. Res.*, *105*(A4), 7509–7519.

Chane, E., B. Van der Holst, C. Jacobs, S. Poedts, and D. Kimpe (2006), Inverse and normal coronal mass ejections: Evolution up to 1 AU, *Astron. Astrophys.*, *447*, 727–733, doi:10.1051/0004-6361:20053802.

Chane, E., S. Poedts, and B. Van der Holst (2008), On the combination of ACE data with numerical simulations to determine the initial characteristics of a CME, *Astron. Astrophys.*, *492*, L29–L32.

Chen, P. F., and K. Shibata (2000), An emerging flux trigger mechanism for coronal mass ejections, *Astrophys. J.*, *545*, 524–531.

Cohen, O., I. V. Sokolov, I. I. Roussev, N. Lugaz, W. B. Manchester, T. I. Gombosi, and C. N. Arge (2008), Validation of a global 3D heliospheric model with observations for the May 12, 1997 CME event, *J. Atmos. Sol. Terr. Phys.*, *70*, 583–592.

Cranmer, S. R. (2002), Coronal holes and the high-speed solar wind, *Space Sci. Rev.*, *101*, 229–294.

Dedner, A., F. Kemm, D. Kroner, C. D. Munz, T. Schnitzer, and M. Wesenberg (2002), Hyperbolic divergence cleaning for the MHD equations, *J. Comput. Phys.*, *175*, 645–673.

Detman, T. R., M. Dryer, T. Yeh, S. M. Han, S. T. Wu, and D. J. McComas (1991), A time-dependent, three-dimensional MHD numerical study of interplanetary magnetic draping around plasmoids in the solar wind, *J. Geophys. Res.*, *96*(A6), 9531–9540.

Dryer, M. (1994), Interplanetary studies: Propagation of disturbances between the Sun and the magnetosphere, *Space Sci. Rev.*, *67*(3/4), 363–419.

Dryer, M. (2007), Space weather simulation in 3D MHD from the Sun to the Earth and beyond to 100 AU: A modeler's perspective of the present state of the art, *Asia J. Phys.*, *16*, 97–121.

Dulk, G. A., Y. Leblanc, and J. L. Bougeret (1999), Type II shock and CME from the corona to 1 AU, *Geophys. Res. Lett.*, *26*(15), 2331–2334.

Eto, S., et al. (2002), Relation between a Moreton wave and an EIT wave observed on 1997 November 4, *Publ. Astron. Soc. Jpn.*, *54*, 481–491.

Evans, C. R., and J. F. Hawley (1988), Simulation of general relativistic magnetohydrodynamic flows: A constrained transport method, *Astrophys. J.*, *332*, 659–677.

Farrugia, C. J., V. A. Osherovich, and L. F. Burlaga (1995), Magnetic flux rope versus the spheromak as models for interplanetary magnetic clouds, *J. Geophys. Res.*, *100*(A7), 12,293–12,306.

Feng, X. S., Y. Q. Hu, and F. S. Wei (2006a), Modeling the resistive MHD by the CESE method, *Sol. Phys.*, *235*, 235–257.

Feng, X. S., Y. F. Zhou, and Y. Q. Hu (2006b), A 3rd order WENO GLM-MHD scheme for magnetic reconnection, *Chin. J. Space Sci.*, *26*(1), 1–7.

Feng, X. S., Y. F. Zhou, and S. T. Wu (2007), A novel numerical implementation for solar wind modeling by the modified conservation element/solution element method, *Astrophys. J.*, *655*, 1110–1126.

Feng, X. S., L. P. Yang, C. Q. Xiang, S. T. Wu, Y. F. Zhou, and D. K. Zhong (2010), Three-dimensional solar wind modeling from the Sun to Earth by a SIP-CESE MHD model with a six-component grid, *Astrophys. J.*, *723*, 300–319.

Feng, X. S., C. Q. Xiang, and D. K. Zhong (2011a), The state-of-art of three-dimensional numerical study for corona-interplanetary process of solar storms, *Sci. Sin-Terrae*, *41*, 1–28.

Feng, X. S., S. H. Zhang, C. Q. Xiang, L. P. Yang, C. W. Jiang, and S. T. Wu (2011b), A hybrid solar wind model of the cese + hll method with a yin-yang overset grid and an AMR grid, *Astrophys. J.*, *734*(1), 50, doi:10.1088/0004-637X/734/1/50.

Feynman, J., and S. F. Martin (1995), The initiation of coronal mass ejections by newly emerging magnetic flux, *J. Geophys. Res.*, *100*, 3355–3367.

Forbes, T. G., E. R. Priest, and P. A. Isenberg (1994), On the maximum energy releasein flux-rope models of eruptive flares, *Sol. Phys.*, *150*, 245.

Gibson, S. E., and Y. Fan (2008), Partially ejected flux ropes: Implications for interplanetary coronal mass ejections, *J. Geophys. Res.*, *113*, A09103, doi:10.1029/2008JA013151.

Gombosi, T. I., D. L. De Zeeuw, K. G. Powell, A. J. Ridley, I. V. Sokolov, Q. F. Stout, and G. Toth (2003), Adaptive mesh refinement for global magnetohydrodynamic simulation, *Lect. Notes Phys.*, *615*, 247–274.

Gosling, J. T., P. Riley, D. J. McComas, and V. J. Pizzo (1998), Overexpanding coronal mass ejections at high heliographic latitudes: Observations and simulations, *J. Geophys. Res.*, *103*(A2), 1941–1954.

Groth, C. P. T., D. L. DeZeeuw, T. I. Gombosi, and K. G. Powell (2000), Global three-dimensional MHD simulation of a space weather event: CME formation, interplanetary propagation, and interaction with the magnetosphere, *J. Geophys. Res.*, *105*, 25,053–25,078.

Hayashi, K., X. P. Zhao, and Y. Liu (2006), MHD simulation of two successive interplanetary disturbances driven by cone-model parameters in IPS-based solar wind, *Geophys. Res. Lett.*, *33*, L20103, doi:10.1029/2006GL027408.

Hollweg, J. V., and P. A. Isenberg (2002), Generation of the fast solar wind: A review with emphasis on the resonant cyclotron interaction, *J. Geophys. Res.*, *107*(A7), 1147, doi:10.1029/2001JA000270.

Kataoka, R., T. Ebisuzaki, K. Kusano, D. Shiota, S. Inoue, T. T. Yamamoto, and M. Tokumaru (2009), Three-dimensional MHD modeling of the solar wind structures associated with 13 December 2006 coronal mass ejection, *J. Geophys. Res.*, *114*, A10102, doi:10.1029/2009JA014167.

Kleimann, J., A. Kopp, H. Fichtner, and R. Grauer (2009), A novel code for numerical 3-D MHD studies of CME expansion, *Ann. Geophys.*, *27*, 989–1004.

Levine, R. H., M. D. Altschuler, and J. W. Harvey (1977), Solar sources of the interplanetary magnetic field and solar wind, *J. Geophys. Res.*, *82*(7), 1061–1065.

Li, X., Q. M. Lu, and B. Li (2007), Ion pickup by finite amplitude parallel propagating Alfvén waves, *Astrophys. J.*, *661*, L105–L108.

Lu, Q. M., and L. Chen (2009), Ion heating by a spectrum of obliquely propagating low-frequency Alfvén waves, *Astrophys. J.*, *704*, 743–749.

Lugaz, N., W. B. Manchester IV, and T. I. Gombosi (2005), Numerical simulation of the interaction of two coronal mass ejections from Sun to Earth, *Astrophys. J.*, *634*, 651–662.

Lugaz, N., W. B. Manchester IV, I. I. Roussev, G. Toth, and T. I. Gombosi (2007), Numerical investigation of the homologous coronal mass ejection events from active region 9236, *Astrophys. J.*, *659*, 788–800.

Lugaz, N., I. I. Roussev, I. V. Sokolov, and C. Jacobs (2010), Solar-terrestrial simulations of CMEs with a realistic initiation mechanism: Case study for Active Region 10069, *AIP Conf. Proc.*, *1216*, 440–443, doi:10.1063/1.3395898.

Luhmann, J. G., Y. Li, C. N. Arge, P. R. Gazis, and R. Ulrich (2002), Solar cycle changes in coronal holes and space weather cycles, *J. Geophys. Res.*, *107*(A8), 1154, doi:10.1029/2001JA007550.

Lynch, B. J., Y. Li, A. F. R. Thernisien, E. Robbrecht, G. H. Fisher, J. G. Luhmann, and A. Vourlidas (2010), Sun to 1 AU propagation and evolution of a slow streamer-blowout coronal mass ejection, *J. Geophys. Res.*, *115*, A07106, doi:10.1029/2009JA015099.

Manchester, W. B., IV, T. I. Gombosi, I. Roussev, D. L. De Zeeuw, I. V. Sokolov, K. G. Powell, and G. Toth (2004a), Three-dimensional MHD simulation of a flux rope driven CME, *J. Geophys. Res.*, *109*, A01102, doi:10.1029/2002JA009672.

Manchester, W. B., IV, T. I. Gombosi, I. Roussev, A. Ridley, D. L. De Zeeuw, I. V. Sokolov, K. G. Powell, and G. Toth (2004b), Modeling a space weather event from the Sun to the Earth: CME generation and interplanetary propagation, *J. Geophys. Res.*, *109*, A02107, doi:10.1029/2003JA010150.

Manchester, W. B., IV, A. J. Ridley, T. I. Gombosi, and D. L. DeZeeuw (2006), Modeling the Sun-to-Earth propagation of a very fast CME, *Adv. Space Res.*, *38*, 253–262.

Manchester, W. B., IV, A. Vourlidas, G. Toth, N. Lugaz, I. I. Roussev, I. V. Sokolov, T. I. Gombosi, D. L. De Zeeuw, and M. Opher (2008), Three-dimensional MHD simulation of the 2003 October 28 coronal mass

ejection: Comparison with LASCO coronagraph observations, *Astrophys. J.*, *684*, 1448–1460.
Mignone, A., and P. Tzeferacos (2010), A second-order unsplit Godunov scheme for cell-centered MHD: The CTU-GLM scheme, *J. Comput. Phys.*, *229*, 2117–2138.
Mikic, Z., and J. A. Linker (1994), Disruption of coronal magnetic field arcades, *Astrophys. J.*, *430*, 898–912.
Nakamizo, A., T. Tanaka, Y. Kubo, S. Kamei, H. Shimazu, and H. Shinagawa (2009), Development of the 3-D MHD model of the solar corona-solar wind combining system, *J. Geophys. Res.*, *114*, A07109, doi:10.1029/2008JA013844.
Odstrcil, D., and V. J. Pizzo (1999), Distortion of the interplanetary magnetic field by three-dimensional propagation of coronal mass ejections in a structured solar wind, *J. Geophys. Res.*, *104*, 28,225–28,239, doi:10.1029/1999JA900319.
Odstrcil, D., and V. J. Pizzo (2009), Numerical heliospheric simulations as assisting tool for interpretation of observations by STEREO heliospheric imagers, *Sol. Phys.*, *259*, 297–309.
Odstrcil, D., J. A. Linker, R. Lionello, Z. Mikic, P. Riley, V. J. Pizzo, and J. G. Luhmann (2002), Merging of coronal and heliospheric numerical two-dimensional MHD models, *J. Geophys. Res.*, *107*(A12), 1493, doi:10.1029/2002JA009334.
Odstrcil, D., P. Riley, and X. P. Zhao (2004), Numerical simulation of the 12 May 1997 interplanetary CME event, *J. Geophys. Res.*, *109*, A02116, doi:10.1029/2003JA010135.
Oginio, T., and R. J. Walker (1984), A magnetohydrodynamic simulation of the bifurcation of tail lobes during intervals with a northward interplanetary magnetic field, *Geophys. Res. Lett.*, *11*(10), 1018–1021, doi:10.1029/GL011i010p01018.
Parker, E. N. (1963), *Interplanetary Dynamical Processes*, Wiley-Interscience, New York.
Powell, K. G., P. L. Roe, T. J. Linde, T. I. Gombosi, and D. L. De Zeeuwy (1999), A solution-adaptive upwind scheme for ideal magnetohydrodynamics, *J. Comput. Phys.*, *154*, 284–309.
Qamar, S., and S. Mudasser (2010), On the application of a variant CE/SE method for solving two-dimensional ideal MHD equations, *Appl. Numer. Math.*, *60*, 587–606.
Riley, P., J. T. Gosling, and V. J. Pizzo (1997), A two-dimensional simulation of the radial and latitudinal evolution of a solar wind disturbance driven by a fast, high-pressure coronal mass ejection, *J. Geophys. Res.*, *102*, 14,677–14,685.
Riley, P., J. T. Gosling, and V. J. Pizzo (2001), Investigation of the polytropic relationship between density and temperature within interplanetary coronal mass ejections using numerical simulations, *J. Geophys. Res.*, *106*(A5), 8291–8300.
Shen, F., X. S. Feng, S. T. Wu, and C. Q. Xiang (2007), Three-dimensional MHD simulation of CMEs in three-dimensional background solar wind with self-consistent structure on the source surface as input: Numerical simulation of the January 1997 Sun-Earth connection event, *J. Geophys. Res.*, *112*, A06109, doi:10.1029/2006JA012164.
Shen, F., X. S. Feng, and W. B. Song (2009), An asynchronous and parallel time-marching method: Application to three-dimensional MHD simulation of solar wind, *Sci. China*, *Ser. E Tech. Sci.*, *52*(10), 2895–2902, doi:10.1007/s11431-009-0291-1.
Stone, J. M., and T. Gardiner (2009), A simple unsplit Godunov method for multidimensional MHD, *New Astron.*, *14* 139–148.
Tanaka, T. (1994), Finite volume TVD scheme on an unstructured grid system for three-dimensional MHD simulation of inhomogeneous systems including strong background potential field, *J. Comput. Phys.*, *111*, 381–389.
Toth, G. (2000), The $\nabla \cdot \mathbf{B}$ constraint in shock-capturing magnetohydroynamics codes, *J. Comput. Phys.*, *161*, 605–652.
Toth, G., D. L. De Zeeuw, T. I. Gombosi, and K. G. Powell (2006), A parallel explicit/implicit time stepping scheme on block-adaptive grids, *J. Comput. Phys.*, *217*, 722–758.
Vandas, M., S. Fischer, P. Pelant, M. Dryer, Z. Smith, and T. Detman (1997), Propagation of a spheromak: 1. Some comparisons of cylindrical and spherical magnetic clouds, *J. Geophys. Res.*, *102*(A11), 24,183–24,193.
Vandas, M., S. Fischer, P. Pelant, M. Dryer, Z. Smith, and T. Detman (1998), Propagation of a spheromak: 2. Three-dimensional structure of a spheromak, *J. Geophys. Res.*, *103*(A10), 23,717–23,725.
Vandas, M., D. Odstrcil, and S. Watari (2002), Three-dimensional MHD simulation of a loop-like magnetic cloud in the solar wind, *J. Geophys. Res.*, *107*(A9), 1236, doi:10.1029/2001JA005068.
Wang, R. S., Q. M. Lu, A. M. Du, and S. Wang (2010a), In situ observations of a secondary magnetic island in an ion diffusion region and associated energetic electrons, *Phys. Rev. Lett.*, *104*, 175003, doi:10.1103/PhysRevLett.104.175003.
Wang, R. S., Q. M. Lu, X. Li, C. Huang, and S. Wang (2010b), Observations of energetic electrons up to 200 keV associated with a secondary island near the center of an ion diffusion region: A Cluster case study, *J. Geophys. Res.*, *115*, A11201, doi:10.1029/2010JA015473.
Wang, Y. M., C. L. Shen, S. Wang, and P. Z. Ye (2004), Deflection of coronal mass ejection in the interplanetary medium, *Sol. Phys.*, *222*, 329–343.
Wu, C.-C., C. D. Fry, S. T. Wu, M. Dryer, and K. Liou (2007), Three-dimensional global simulation of interplanetary coronal mass ejection propagation from the Sun to the heliosphere: Solar event of 12 May 1997, *J. Geophys. Res.*, *112*, A09104, doi:10.1029/2006JA012211.
Wu, S. T., W. P. Guo, D. J. Michels, and L. F. Burlaga (1999), MHD description of the dynamical relationships between a flux rope, streamer, coronal mass ejection, and magnetic cloud: An analysis of the January 1997 Sun-Earth connection event, *J. Geophys. Res.*, *104*, 14,789–14,801.
Wu, S. T., T. X. Zhang, E. Tandberg-Hanssen, Y. Liu, X. S. Feng, and A. Tan (2005), Numerical magnetohydrodynamic experiments for testing the physical mechanisms of coronal mass ejections acceleration, *Sol. Phys.*, *225*, 157–175.
Yalim, M. S., D. Vanden Abeele, A. Lani, T. Quintino, and H. Deconinck (2011), A finite volume implicit time integration method for solving the equations of ideal magnetohydrodynamics for the hyperbolic divergence cleaning approach, *J. Comput. Phys.*, *230*, 6136–6154, doi:10.1016/j.jcp2011.04.020.
Yang, L. P., X. S. Feng, C. Q. Xiang, S. H. Zhang, and S. T. Wu (2011), Simulation of the unusual solar minimum with 3D SIP-CESE MHD model by comparison with multi-satellite observations, *Sol. Phys.*, *271*, 91–110.
Zhang, J., J. Wang, Y. Deng, and D. Wu (2001), Magnetic flux cancellation associated with the major solar event on 2000 July 14, *Astrophys. J.*, *548*, L99–L102.
Zhang, M., S. T. Yu, S. C. Lin, S. C. Chang, and I. Blankson (2006), Solving the MHD equations by the space-time conservation element and solution element method, *J. Comput. Phys.*, *214*, 599–617.
Zhou, Y. F., and X. S. Feng (2008), Numerical study of successive CMEs during November 4–5, 1998, *Sci. China Ser. E Tech. Sci.*, *51*(10), 1600–1610.
Zhou, Y. F., X. S. Feng, and S. T. Wu (2008), Numerical simulation of the 12 May 1997 CME event, *Chin. Phys. Lett.*, *25*(2), 790–792.

D. Du, National Center for Space Weather, CMA, Beijing 100081, China. (dud@cma.gov.cn)
X. S. Feng, F. Shen, C. Q. Xiang, and Y. F. Zhou, SIGMA Weather Group, State Key Laboratory of Space Weather, Center for Space Science and Applied Research, Chinese Academy of Science, Beijing 100190, China. (fengx@sapceweather.ac.cn; fshen@spaceweather.ac.cn; cqxiang@spaceweather.ac.cn; yfzhou@spaceweather.ac.cn)
S. T. Wu, Center for Space Plasma and Aeronomic Research, University of Alabama, Huntsville, AL 35899, USA. (wus@cspar.uah.edu)